

# Human adaptive tracking and localization in Logistic Operations

Federica Pascucci <sup>1</sup>, Marco Dolfi <sup>2</sup>, Simone Morosi <sup>2</sup>, Laura Giarré <sup>3</sup>

**Abstract**—Modern logistic operations in warehouses consist of human and robots working in the same large indoor or outdoor areas. To design safe and efficient area and avoid collisions or accidents, localization and tracking of humans need to be deployed. The development of location based service, such as human activity monitoring, has been one of the drivers for the last decade interest in indoor or outdoor positioning and localization. In this work, a novel tracking system integrating inertial measurements and an ultra-wide band infrastructure is proposed to follow and localize humans in a warehouse scenario. The system has been designed to be self-configurable, able to learn online most of the needed parameters. Being the computational load low, it can be implemented on wearable devices. We tested the tracking system in a real outdoor scenario where the adaptive online algorithms have shown their effectiveness and improvements with respect to existing approaches.

## I. INTRODUCTION AND STATE OF THE ART

Modern warehouse and logistic operations consist of large indoor or outdoor areas where robots are transferring goods, moving racks, and performing physically difficult and repetitive tasks. This is performed near humans, whose presence may affect the operations and warehouse efficiency. So, there is a need of implementing some safety system that requires the human localization as one of its essential components. In the present paper we focus our attention to the human localization and tracking, designing a novel solution to perform an improved positioning system for monitoring persons in logistic operation areas. Indoor or outdoor localization is very important in many fields, such as robotics, assistive technology, tourism, industrial monitoring ([1], [2]), sport ([3], [4]), and in high risk operations (e.g., firefighters interventions [5]). Two methods for monitoring human motion or determining pedestrian position have recently gained attentions, the Pedestrian Dead Reckoning (PDR) using the inertial sensors and localization methods using an UWB (Ultra Wide Band) infrastructure. The process of estimating the position of humans using inertial sensors is referred to as PDR and it is widely used when GPS fails (like in an indoor environment) or when it is unavailable or its accuracy is not sufficient, although the results may not be accurate. Inertial sensors present in many applications some limitations due to drifts. In [6] an analysis of available PDR methods with

a focus on wearable sensors is presented and a comparison of the accuracy of different sensor layouts and algorithms is shown. The UWB framework presented in [7] and [8] use a set of static UWB receivers, named anchors, playing the role of receivers together with some UWB transmitter (in the wearable device). The UWB communication link from the on-body transmitter to the receivers can be influenced by many factors such as the relative height between the transmitting and the receiving antennas as shown in [4], [9].

The novel positioning system presented in this paper is improving the performance of the UWB by integrating a PDR localization system, using wearable sensors. Integration of UWB and PDR algorithms has been proposed for outdoor scenarios in [3] and for indoor applications in [10], using a Kalman (extended or, respectively, unscented) filter for the sensor fusion operations. To estimate the state of the PDR and UWB fusion system is commonly use a Kalman filter exploiting the prior information on the data covariance matrix (see [11], [12]). In [13] a robust nonlinear Kalman is implemented to overcome both the challenges encountered by the UWB (nonline-of-sight conditions) and the error accumulation of PDR. Here, We fuse the two localization methods to improve performance and positioning accuracy, indoor or outdoor. The key features and novelty of the presented *sensor fusion algorithm* with respect to previous contributions [3], [4] can be summarized as follows:

- 1) All model parameters are identified and estimated online, so the algorithm is independent from the user (i.e., weight, gender, height) and from the system calibration (i.e., accelerometer bias, positions of the anchors, magnetometer calibration, and so on). No a priori knowledge of the human body size is required.
- 2) A recursive parameter estimation via an adaptive learning procedure is presented.
- 3) The online algorithm estimates two human activities: standing still and motion (slowly walking and fastly walking). Despite previous attempt to solve this problem, this can be done now because the parameter related to the human walking step length is estimated at each run of the algorithm with no body information.
- 4) The algorithm is low time consuming.

To evaluate the performance of the localization algorithm there certain criteria need to be satisfied. A first attempt to standardize such tests to be passed to evaluate the localization systems was the ISO/IEC 18305 standard, see [14] where the various evaluation standard methodologies are compared. We refer to such standard to define our tests and comparisons at system level, and further key performance indicators have

<sup>3</sup>Laura Giarré is with the Engineering Department 'Enzo Ferrari', University of Modena and Reggio Emilia, Modena, Italy. [lagiarre@unimore.it](mailto:lagiarre@unimore.it)

<sup>1</sup>Federica Pascucci is with Department of ICITA, University of Roma Tre, Rome, Italy [federica.pascucci@uniroma3.it](mailto:federica.pascucci@uniroma3.it).

<sup>2</sup>Marco Dolfi e Simone Morosi are with the Department of Information Engineering, University of Florence, Firenze, Italy [marco.dolfi@unifi.it](mailto:marco.dolfi@unifi.it), [simone.morosi@unifi.it](mailto:simone.morosi@unifi.it)

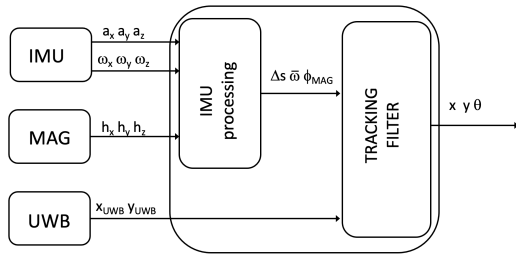


Fig. 1. Tracking system architecture

been evaluated.

The paper is organized as follows: in Section II the adopted tracking system is detailed while in Section III the processing of the data collected by the inertial sensors is described. In Section IV the filter used for tracking is highlighted. Finally, in Section V the achieved results are reported. In Section VI the conclusive remarks are drawn.

## II. TRACKING SYSTEM DESCRIPTION

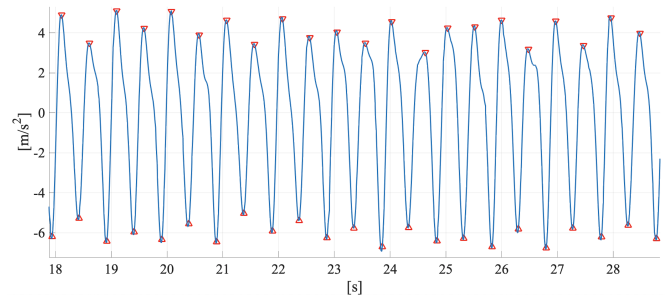
The tracking system has been developed to compute the position of a person in an industry environment or warehouse. We focus the present paper and the tests on an outdoor area, but indoor tests are also ongoing. The human is equipped with a wearable device, consisting of an Inertial Measurement Unit (IMU), a magnetometer, and an UWB blinker. A set of UWB anchors are deployed on the perimeter of the area of interest. Thus, the output of the tracking system is the vector  $\hat{x}_i$  composed by the position coordinates and the orientation of the human in a 2D environment.

All sensors provide information about the person movement: the IMU can compute the accelerations and the angular velocities, the magnetometer reports the orientation, and the UWB system can retrieve the position. The latter at each time instant is computed according to the architecture sketched in Fig.1. The data provided by the IMU are pre-processed to retrieve the displacement of the person during a sampling interval. This information is used to build a prediction of the human position and orientation. The prediction is further adjusted by the information provided by the magnetometer and the UWB positioning system.

It is worth noticing that i) the IMU and magnetometer data are measured according to a moving coordinate frame, i.e. the IMU *body frame* (BF); ii) the UWB data are computed with respect to a fixed coordinate frame, i.e., the *global frame* (GF). Therefore, a transformation from BF to GF according to the IMU orientation has to be applied to merge the information from the different sensors.

## III. DATA ELABORATION WITH IMU AND MAGNETOMETER PROCESSING

Processing the data collected by the IMU and magnetometer is necessary to estimate the displacement and orientation of the human. In this contribution, we assume that the human stands still, slowly walks, or fastly walks in the considered area. The wearable device is placed on the back of the

Fig. 2. Acceleration coronal axes of the human, triangles point  $a_M$  and  $a_m$  during a walking step event

person, near the center of mass, having the vertical axis of the BF aligned with the human coronal plane, perpendicular to the area. This position of the the device provides several advantages resulting in a reduced computational complexity. In more details, concerning accelerometers, only data along  $z$ -axis of the BF need to be processed. The orientation can be computed by integrating the gyroscopes data along the same axis. The heading from magnetometer is computed using data in the transversal plane of the user, i.e., data on the  $x, y$ -plane of the BF. Since the  $z$ - axes of BF and GF are aligned, the transformation from BF to GF reduces to an orientation shift, once the initial position and orientation of the human with respect to the GF are known.

### A. Activity detection

The human activities considered in this work are *standing still* and *motion*. A set of samples from the accelerometer and gyroscope is analyzed to detect different activities. Specifically, the covariance of the set of measurements is computed and compared with the thresholds

$$\text{cov}(m_j, m_{j+1}, \dots, m_{j+k}) \leq t_m \quad (1)$$

where  $m_j$  is the measurement and  $t_m$  is the correspondent threshold.

If one of the covariance values is lower than the threshold, the activity is classified as *standing still*, otherwise *motion*. The parameters  $t_m$  is fixed, while the cardinality of the measurement sets  $k$  is updated during the experiment. It is worth noticing that a covariance computed over a large number of measurements is more accurate, however this may introduce a delay in the position computation. Therefore, the choice of  $k$  represents a trade-off between accuracy and delay. This choice is based on the activity motion: specifically,

$$k = 3l \quad (2)$$

where  $l$  is the number of measurement samples retrieved during a single walking step event.

### B. Adaptive bias computation

The main source of errors using IMU is biases affecting both accelerometers and gyroscopes. The bias is often removed by the pre-processing done by the sensor. However, since the bias changes slowly over time due to different

operational conditions (e.g., the temperature), a constant residual error always affects the data. To remove it, the measurements collected during *standing still* are used to estimate the bias:

$$b = \text{avg}(m_j, m_{j+1}, \dots, m_{j+k}). \quad (3)$$

Once estimated, the bias is eliminated from the corresponding measurement. Following this approach, the gravitational acceleration is also removed since it can be considered as a bias along the  $z$ -axis of the BF.

### C. Adaptive displacement computation

There are several methods to compute the displacement over a time interval by processing the IMU data. Here, the integration of the accelerometer signal is not considered, as it has been proven to be inaccurate and requires all the accelerometer components. To determine the walking step length, the dynamic approach proposed in [15] is considered, thus the displacement  $\Delta s$  at each walking step event  $n$  becomes

$$\Delta s_n = \beta \sqrt[4]{a_{M,n} - a_{m,n}} \quad (4)$$

where  $\beta$  is a parameter that depends on gender, weight, and height of the person, while  $a_{M,n}$  and  $a_{m,n}$  are the maximum and minimum accelerations along the  $z$ -axis of the GF retrieved during the walking step event  $n$ . The displacement depends on the accelerations in the event, which change when the human is slowly walking or fastly walking: this allows to reduce the number of activities to be recognized during the detection phase. On the other hand, the  $a_{M,n}$  and  $a_{m,n}$  are known once a single walking step event is isolated.

A walking step is identified by  $l$  samples; however, this number changes due to the speed of movement, this is why we use an adaptive algorithm to online compute it. At the beginning of the procedure,  $l$  is initialized by considering the IMU sampling frequency and the average step frequency in human walking (i.e., 1.5Hz). Afterwards,  $k$  samples are collected to perform activity identification. If *motion* is detected, the accelerometer data is prefiltered using a low pass filter to remove high frequency noise. The two phases of the gait cycle (i.e., double limb and single limb support) produce a peak and valley around zero in the acceleration along the coronal axis, as shown in Fig. 2. The adaptive algorithm identifies two adjacent zero crossings and computes  $a_{M,n}$  and  $a_{m,n}$ . These acceleration values are used to set the adaptive thresholds  $p_a = 0.8a_{M,n}$  and  $v_a = 0.8a_{m,n}$ . These thresholds are applied to the  $k$  accelerometer samples to identify the walking steps. Once the walking steps are identified, the number  $l$  of acceleration samples is updated as the mean value of the samples in each walking step. It is worth noticing that when the human changes activity, some walking steps cannot be correctly classified; however, in this case, once the change is recognized, a post-processing of the signal is performed.

Because we need to obtain a tuning that is human-independent, the parameter  $\beta$  is initialized once the first *motion* activity is detected. The distance computed by the

UWB positioning system and the maximum and minimum accelerations are used to compute the a sequence  $\beta_n$ ; the parameter is computed as

$$\beta = \text{avg}(\beta_1, \beta_2, \dots, \beta_n) \quad (5)$$

### D. Adaptive magnetometer calibration

Consumer-grade magnetometers are prone to several errors. According to [16], these errors can be divided into instrumentation errors and magnetic deviation. The former depend on the device and are represented by scale factors, bias, and non-orthogonality of the axes. The magnetic deviations depends on the ferromagnetic features of the environment. They can be classified as hard iron and soft iron: the first can be modeled as bias, the second as scale factor.

By combined the instrumentation errors and the magnetic deviation, the vector of measurements  $\mathbf{h}_m$  retrieved by the magnetometer can be written as

$$\mathbf{h}_E = \mathbf{C}\mathbf{h}_m + \mathbf{g} \quad (6)$$

where  $\mathbf{h}_E$  is the vector of the Earth magnetic field, the matrix  $\mathbf{C}$  encodes the scale factors, the non-orthogonality and the soft iron errors, and  $\mathbf{g}$  is the vector of the bias and hard iron errors. When magnetometer measurements are not affected by perturbations, the norm of the magnetometer vector is equal to the magnitude of the Earth's magnetic field. When the magnetometer rotates in space, the collected measurements should lie on a ellipsoid. Considering this constraint, the calibration parameters, i.e., the matrix  $\mathbf{C}$  and the vector  $\mathbf{g}$ , can be easily retrieved by using an ellipsoid fitting algorithm [17]. Considering only the measurement in the  $(x, y)$ -plane of the BF, the calibration reduces to finding the parameter that fits a ellipse, as shown in Fig. 3.

To calibrate the magnetometer, there is a need of collecting a number of measurements retrieved at different heading angles, to avoid unstable calibration. Thus, the magnetometer is used in the tracking filter only when the calibration is stable, i.e., the calibration parameters do not vary significantly when new measurements are available. Once the magnetometer is calibrated, a post processing can be performed to further improve the accuracy of the heading. The magnetometer measurements on  $(x, y)$ -plane provide the orientation of human as

$$\varphi_{i,MAG} = \text{atan2}(\hat{h}_{m,y}/\hat{h}_{m,x}) \quad (7)$$

where  $\hat{h}_{m,x}$  and  $\hat{h}_{m,y}$  represent the calibrated measurement of the magnetometer.

## IV. TRACKING FILTER

The tracking filter collects the data from different sensors and provides the position and orientation  $\hat{\mathbf{x}}_i = [\hat{x}_i, \hat{y}_i, \hat{\theta}_i]^T$  of the user every time a walking step event  $i$  is detected. The sensor fusion among IMU, magnetometer, and UWB positioning system is implemented by an Extended Kalman Filter (EKF). As mentioned above, in the prediction step, IMU data are used to perform PDR. In the correction step,

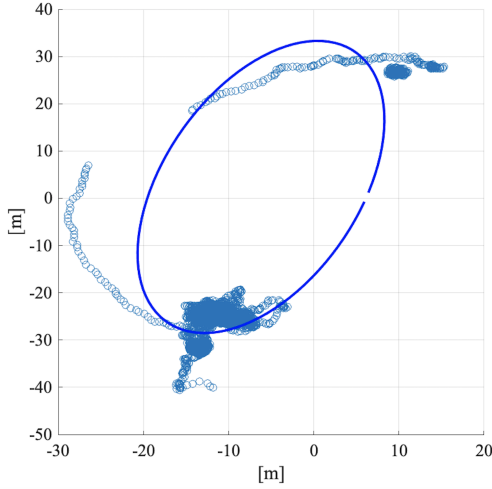


Fig. 3. Calibration ellipse for magnetometer. The area around the user is depicted in meters.

magnetometer and UWB positioning refine this estimate. Since the data are not synchronized with walking step events, the update of the estimate is not always performed. Therefore, we consider two separate correction stages, the first for the magnetometer and the second for the UWB positioning system.

Positioning algorithms based on PDR assume that the starting position and orientation is known. Most of the time this assumption are unrealistic. Here, we consider as starting position and orientation the one computed by the UWB system during the calibration of IMU and magnetometer. Once reliable data from magnetometer are available, the orientation from the Earth reference frame to the GF can be obtained by a shift.

#### A. PDR prediction

The classical *Kalman prediction* step is computed hereafter by updating the state composed by the position  $s$  and the orientation  $\theta$  of the person according to the displacement  $\Delta s$  computed in the walking step event and the angular velocity  $\omega$  from the gyroscopes, specifically

$$\begin{aligned}\hat{\mathbf{x}}_{i|i-1} &= \mathbf{f}(\hat{\mathbf{x}}_{i-1|i-1}, \bar{\omega}_i) = \\ &= \mathbf{A}\hat{\mathbf{x}}_{i-1|i-1} + \begin{bmatrix} \Delta s_i \cos \theta_{i-1|i-1} \\ \Delta s_i \sin \theta_{i-1|i-1} \\ (\bar{\omega}_i - b_\omega)\Delta t_i \end{bmatrix} \\ \mathbf{P}_{i|i-1} &= \mathbf{J}_x^f \mathbf{P}_{i-1|i-1} \mathbf{J}_x^{fT} + \mathbf{Q}_i\end{aligned}\quad (8)$$

where  $\mathbf{A} = \mathbf{I}_{3 \times 3}$ ,  $\bar{\omega}_i$  is the mean angular velocity computed on the samples collected during the walking step event,  $\Delta t_i$  is the duration of the walking step event,  $\mathbf{P}_{i|i-1}$  is the prediction covariance matrix, and  $\mathbf{J}_x^f$  is the Jacobian of  $\mathbf{f}(\cdot)$  with respect to  $\hat{\mathbf{x}}$ .

#### B. Magnetometer correction

The magnetometer provides information about the orientation of the person,  $\varphi_{i,M}$ . Thus, the expected measurement

can be modeled as

$$\hat{y}_i = \mathbf{C} \hat{\mathbf{x}}_{i|i-1} = [0 \ 0 \ 1] \hat{\mathbf{x}}_{i|i-1}. \quad (9)$$

The classical *Kalman update* equations can be written in the presented context as

$$\begin{aligned}s_i &= \mathbf{C} \mathbf{P}_{i|i-1} \mathbf{C}^T + r_i \\ \mathbf{k}_i &= \mathbf{P}_{i|i-1} \mathbf{C}^T s_i^{-1} \\ \hat{\mathbf{x}}_{i|i} &= \hat{\mathbf{x}}_{i|i-1} + \mathbf{k}_i (\varphi_{i,M} - \mathbf{C} \hat{\mathbf{x}}_{i|i-1}) \\ \mathbf{P}_{i|i} &= (\mathbf{I}_{3 \times 3} - \mathbf{k}_i \mathbf{C}) \mathbf{P}_{i|i-1}\end{aligned}\quad (10)$$

where  $r_i$  is the covariance that model the uncertainties of the magnetometer measurements.

#### C. UWB correction

The UWB system implements a remote positioning configuration: the tracked human wears a blinker, that transmits a ranging signal to the anchors on the perimeter. The anchors are deployed along the area and are self configurable. Once the anchors are placed, a calibration algorithm is able to find their positions with respect to a reference framework having its origin in the position of one anchor, labelled as 1, the  $x$ -axis heading to an adjacent anchor, labelled 2 and the  $y$ -axis so to have a Cartesian reference frame. This frame represents the GF of the tracking system.

The anchors can compute the distance from the human exploiting the time-of-flight of the signal. All the distances computed by the anchors are forwarded to a master station that is able to retrieve the position of the user. In particular, a multi-lateration algorithm is used to find the position of the person in the GF. In a 2D environment, such as a flat area, the exact position of the blinker ( $x_{i,UWB}, y_{i,UWB}$ ) is completely defined using three anchors; however, the exploitation of a greater number of anchors can further improve the accuracy of the measurement.

Moreover, the UWB system can be used to also provide information on the orientation of the human by computing the heading angle as

$$\varphi_{i,UWB} = \text{atan2}\left(\frac{y_{i,UWB} - y_{i-1,UWB}}{x_{i,UWB} - x_{i-1,UWB}}\right) \quad (11)$$

Note that the heading angles  $\phi$  and  $\theta$  are named differently because they are measured with very different sampling time.

The information provided by the UWB system, i.e., the position and the orientation of the person  $\mathbf{x}_{i,UWB} = [x_{i,UWB}, y_{i,UWB}, \varphi_{i,UWB}]^T$  is used in the *Kalman correction step* of the tracking filter according to the following equations:

$$\begin{aligned}\mathbf{S}_i &= \mathbf{P}_{i|i-1} + \mathbf{R}_i \\ \mathbf{K}_i &= \mathbf{P}_{i|i-1} \mathbf{S}_i^{-1} \\ \hat{\mathbf{x}}_{i|i} &= \hat{\mathbf{x}}_{i|i-1} + \mathbf{K}_i (\mathbf{x}_{i,UWB} - \hat{\mathbf{x}}_{i|i-1}) \\ \mathbf{P}_{i|i} &= (\mathbf{I}_{3 \times 3} - \mathbf{K}_i) \mathbf{P}_{i|i-1}\end{aligned}\quad (12)$$

where  $\mathbf{R}_i$  is the covariance matrix that model the uncertainties of the UWB measurements.

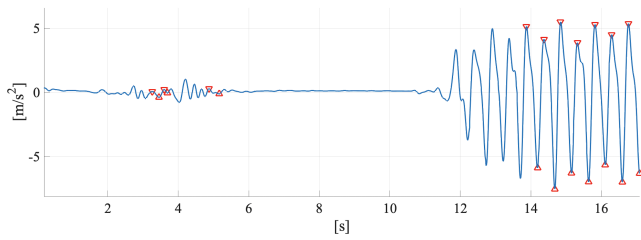


Fig. 4. Acceleration along coronal axes of the human during standing still event, triangles identify false negative

TABLE I  
ACTIVITY DETECTION OUTCOME

True P	False P	True N	False N
259	5	34	7

## V. EXPERIMENTAL RESULTS

The proposed approach has been validated in real scenario. Hereafter, only two significant experiments. The positions retrieved from the UWB system and the data from IMU and magnetometer has been collected during the experiments and have been post-processed by using a Matlab tool developed by the Authors [3].

The UWB positioning system is composed by 6 receivers (anchors) placed on the perimeter of the area, as shown in Fig. 6. The blinker is equipped with the UWB transmitter; both the blinker and the anchors are supplied with a Decawave DWM1000 UWB transceiver and a Li-Po battery-powered, whereas the anchors include also a WiFi module. The blinker is attached to a belt to obtain a waist-mounted configuration. In [4] a full description of the UWB positioning system specifications can be found. Concerning the inertial sensors, an Intel IMU contained in an ASUS ZenPhone 2 has been used. An Android app has been also developed to log the data at the maximum sampling frequency available (i.e., 80Hz). The mobile phone is also placed on the belt, near the center of gravity of the user.

In the first experiment, the human moves from anchor 2 to anchor 5. The human starts the experiment with a standing still activity lasting 15s, then reaches the opposite side, turns back, and stops for 10s. Finally, he comes back to the starting position. The overall length of the path is 50 m. During the experiment, the person changes the walking speed, so the IMU processing needs to adapt the parameters to accurately compute the displacement.

The result of the activity detection is reported in Tab. I, where positive is the activity *motion* and negative is the activity *standing still*. A quantitative analysis is proposed based on the classification error: specifically, the accuracy, the sensitivity, the specificity, the positive predictive value (PPV), and the negative predictive value (NPV) is reported in Tab. II. As it can be seen, the activities are correctly classified and the classifier shows an optimal predictive capability for positive events (i.e., motion), while the standing still activity is more difficult to detect. This is due to i) the limited duration of the standing still activity with respect to the

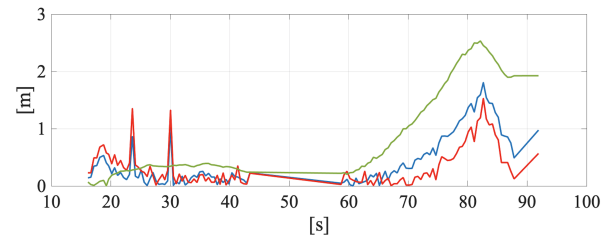


Fig. 5. Error [m] vs time [s]: blue line is the error of the proposed tracking filter, red line of UWB positioning system, and green line PDR

TABLE II  
PERFORMANCES OF THE ACTIVITY DETECTION

Accuracy	Sensitivity	Specificity	PPV	NPV
96%	97%	87%	98%	83%

motion one (i.e., there are less events to be classified as standing still) ii) the residual errors during activity switching. For example, some walking steps are recognized when the user is standing still before start, as highlighted in Fig. 4 due to the adaptive threshold.

The error of human tracking using IMU only, UWB only and the proposed algorithm (PDR+UWB) is shown in Fig. 5. To evaluate the effectiveness of the approach, we analyze the overall trajectory rather than a set of fixed reference points. To this aim, we use a line from anchors 2 to 5 as as ground truth. The distance between the estimated path measures how the its shape is different from the ground truth. In Tab. III we report the error (with its Covariance (COV), Maximum (MAX) and minimum (MIN) value of the path estimated by the PDR, the UWB positioning system, and the fused tracking filter (PDR+UWB). It worth noticing that the maximum error, as well as the mean error is suitably reduced by merging information from different sources. Concerning the maximum error, it occurs in the last part of the path, when the orientation computed by the IMU accumulate errors and the data from UWB are not accurate. Along this segment, indeed, the blinker is able to retrieve few signals from aligned anchors, thus the positioning results less precise. According to ISO/IEC 18305 standard we evaluate the localization error when the user stops and at starting position. When user stops the mean error is about 13 cm. The final localization error is about 90 cm.

In the second experiment, the human moves from the starting position S near 6 to anchor 3. The user starts the experiment with a standing still activity lasting 10s, then reaches the anchor in the opposite corner, turns back, and directly comes back to anchor 6. The overall length of the path is 100 m. Also in this experiment, the user changes the pace and the parameters for activity recognition, walking step detection and length computation are modified accordingly.

The obtained human tracking is reported in Fig. 6. In this case the ground truth is represented by the line intersecting anchor 1 and anchor 5. In Tab. IV are reported the errors retrieved by the different tracking algorithms. The proposed tracking system performs better during this experiment: in

TABLE III  
ERROR COMPARISON

Tracking Algorithm	Mean err[m]	Cov err[m <sup>2</sup> ]	Min err[m]	Max err[m]
PDR	0.84	0.61	0.01	2.53
UWB	0.33	0.11	0.01	1.52
PDR+UWB	0.22	0.10	0.01	1.30

TABLE IV  
ERROR COMPARISON

Tracking Algorithm	Mean err[m]	Cov err[m <sup>2</sup> ]	Min err[m]	Max err[m]
PDR	0.76	0.36	0.03	2.2
UWB	0.76	0.16	0.01	1.78
PDR+UWB	0.49	0.09	0.02	1.50%

this case the UWB anchors are not always aligned to the blinker, so the estimate results more accurate. The PDR results less precise, since the path is longer than the previous one and the inertial estimate accumulates errors. Once this errors are bounded from the UWB positioning system, the overall performance are improved. According to ISO/IEC 18305 standard we evaluate the localization error when the user stops and at starting position. When user reach anchors 3 the error is about 1 m. The final localization error is about 50 cm.

## VI. CONCLUSION

In this contribution a tracking system for human operating in a warehouse has been designed and implemented. The tracking system is able to merge information from inertial sensors and UWB anchors, requiring wearable sensors on the persons and a light infrastructure deployable in the area of interest. The proposed tracking system presents two main advantages. The system is able to learn online all the parameters needed for the computation. The computational load is low, so the algorithm can be easily implemented on an embedded system. The results obtained are promising, however, there is still room for improvements in the human movement detection. Now it is able to classify the motion with high accuracy, however, more different activities need to be recognized. In an operation area, the motion of the people is not limited to slowly walking and fastly walking. Moreover, an improvement can be obtained by differently filtering the collected IMU data to compute the orientation. Its precision, indeed, affects also the position estimate. An integration with obstacle avoidance and safety algorithms with autonomous robots working in the area is the next step of this work.

## REFERENCES

- [1] G. Popović, I. Cvišić, G. Écorchard, I. Marković, L. Přeučil, and I. Petrović, "Human localization in robotized warehouses based on stereo odometry and ground-marker fusion," *Robotics and Computer-Integrated Manufacturing*, vol. 73, p. 102241, 2022.
- [2] S. Proia, G. Cavone, A. Camposeo, F. Ceglie, R. Carli, and M. Dotoli, "Safe and ergonomic human-drone interaction in warehouses," in *2022 IEEE/RSJ International Conference on Intelligent Robots and Systems (IROS)*, 2022, pp. 6681–6686.
- [3] L. Giarré, F. Pascucci, S. Morosi, and A. Martinelli, "Improved pdr localization via uwb-anchor based on-line calibration," in *2018 IEEE 4th International Forum on Research and Technology for Society and Industry (RTSI)*, 2018.

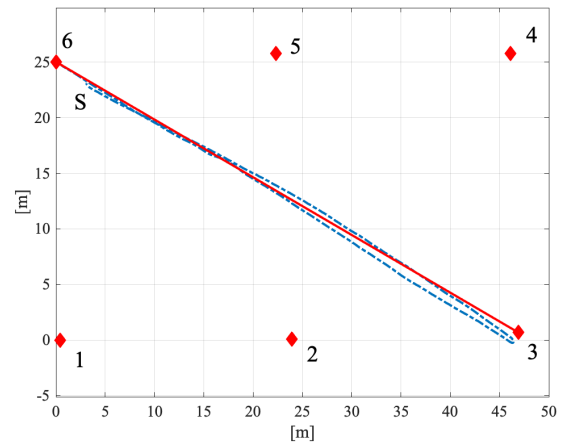


Fig. 6. Trajectory estimated by the proposed algorithm (blue dotted line) and ground truth (red solid line). Diamonds represent the position of the UWB anchors during the experiments. S is the starting point. The trajectory is reported in meters

- [4] A. Martinelli, M. Dolfi, S. Morosi, L. Mucchi, M. Paoli, and A. Agili, "Ultra-wide band positioning in sport: How the relative height between the transmitting and the receiving antenna affects the system performance," *International Journal of Wireless Information Networks*, 2020.
- [5] L. Faramondi, F. Inderst, F. Pascucci, R. Setola, and U. Delprato, "An enhanced indoor positioning system for first responders," in *International Conference on Indoor Positioning and Indoor Navigation*, 2013, pp. 1–8.
- [6] X. Hou and J. Bergmann, "Pedestrian dead reckoning with wearable sensors: A systematic review," *IEEE Sensors Journal*, vol. 21, no. 1, pp. 143–152, 2021.
- [7] K. M. Tan and C. L. Law, "Gps and uwb integration for indoor positioning," in *2007 6th International Conference on Information, Communications & Signal Processing*, 2007, pp. 1–5.
- [8] A. Alarifi, A. Al-Salman, M. Alsaleh, A. Alnafessah, S. Al-Hadhrani, M. A. Al-Ammar, and H. S. Al-Khalifa, "Ultra wideband indoor positioning technologies: Analysis and recent advances," *Sensors*, vol. 16, no. 5, 2016.
- [9] A. Martinelli, M. Dolfi, S. Morosi, L. Mucchi, M. Paoli, and A. Agili, "Ultra-wide band positioning in sport: How the on-body tag location affects the system performance," in *13th EAI International Conference on Body Area Networks*, C. Sugimoto, H. Farhadi, and M. Hämmäläinen, Eds. Springer International Publishing, 2020, pp. 3–16.
- [10] P. Chen, Y. Kuang, and X. Chen, "A uwb/improved pdr integration algorithm applied to dynamic indoor positioning for pedestrians," *Sensors*, vol. 17, no. 9, 2017.
- [11] J. Corrales, F. Candelas, and F. Torres, "Sensor data integration for indoor human tracking," *Robotics and Autonomous Systems*, vol. 58, no. 8, pp. 931–939, 2010.
- [12] J. Lu, K. Chen, B. Li, and M. Dai, "Hybrid navigation method of ins/pdr based on action recognition," *IEEE Sensors Journal*, vol. 18, no. 20, pp. 8541–8548, 2018.
- [13] L. Xin, Y. Wang, and K. Khoshelham, "Uwb/pdr tightly coupled navigation with robust extended kalman filter for nlos environments," *Mobile Information Systems*, 2018.
- [14] D. Bousdar Ahmed, L. E. Diez, E. M. Diaz, and J. J. García Domínguez, "A survey on test and evaluation methodologies of pedestrian localization systems," *IEEE Sensors Journal*, vol. 20, no. 1, pp. 479–491, 2020.
- [15] H. Weinberg, "Using the adxl202 in pedometer and personal navigation applications," Analog Device, Tech. Rep., 2002.
- [16] V. Renaudin, M. Afzal, and G. Lachapelle, "Complete triaxis magnetometer calibration in the magnetic domain," *Journal of Sensors*, 2010.
- [17] A. Fitzgibbon, M. Pilu, and R. Fisher, "Direct least square fitting of ellipses," *IEEE Transactions on Pattern Analysis and Machine Intelligence*, vol. 21, no. 5, pp. 476–480, 1999.